ACS OMEGA

http://pubs.acs.org/journal/acsodf

Article

Visualizing Tetrahedral Oxyanion Bound in HIV-1 Protease Using Neutrons: Implications for the Catalytic Mechanism and Drug Design

Mukesh Kumar, Kalyaneswar Mandal, Matthew P. Blakeley, Troy Wymore, Stephen B. H. Kent, John M. Louis, Amit Das,* and Andrey Kovalevsky*

Cite This: *ACS Omega* 2020, 5, 11605−11617

Read Online

ACCESS | Metrics & More | Article Recommendations | Supporting Information

ABSTRACT: HIV-1 protease is indispensable for virus propagation and an important therapeutic target for antiviral inhibitors to treat AIDS. As such inhibitors are transition-state mimics, a detailed understanding of the enzyme mechanism is crucial for the development of better anti-HIV drugs. Here, we used room-temperature joint X-ray/neutron crystallography to directly visualize hydrogen atoms and map hydrogen bonding interactions in a protease complex with peptidomimetic inhibitor KVS-1 containing a reactive nonhydrolyzable ketomethylene isostere, which, upon reacting with the catalytic water molecule, is converted into a tetrahedral intermediate state, KVS-1_{TI}. We unambiguously determined that the resulting tetrahedral intermediate is an oxyanion, rather than the *gem*-diol, and both catalytic aspartic acid residues are protonated. The oxyanion tetrahedral intermediate appears to be unstable, even though the negative charge on the oxyanion is delocalized through a strong n → π^* hyperconjugative interaction into the nearby peptidic carbonyl group of the inhibitor. To better understand the influence of the ketomethylene isostere as a protease inhibitor, we have also examined the protease structure and binding affinity with keto-darunavir (keto-DRV), which similar to KVS-1 includes the ketomethylene isostere. We show that keto-DRV is a significantly less potent protease inhibitor than DRV. These findings shed light on the reaction mechanism of peptide hydrolysis catalyzed by HIV-1 protease and provide valuable insights into further improvements in the design of protease inhibitors.

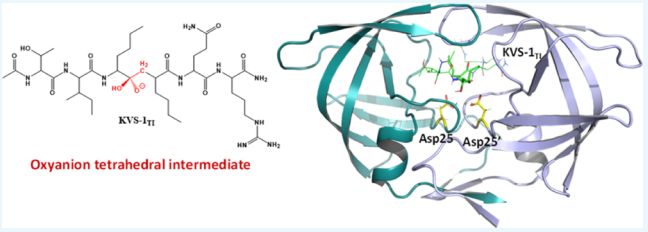

INTRODUCTION

Enzymes ensure the existence of life by dramatically accelerating the rates of many chemical reactions that, if uncatalyzed, may have virtually insurmountable energy barriers. A mechanistic understanding of the remarkable catalytic efficiency of these biomacromolecular catalysts is crucial in designing drugs to battle many human diseases. Human immunodeficiency virus type 1 (HIV-1) that causes AIDS has been in the public eye for almost four decades. Drugs targeting virtually every enzyme of HIV-1 have been designed and further developed into clinical therapeutics,[1,2] essentially transforming this deadly disease into a chronic condition for many patients. In this regard, inhibition of HIV-1 protease (PR) has played a crucial role in improving lives of many infected people.[3,4] The design of protease inhibitors is considered as one of the greatest successes of structure-based drug design.[5] Rapid accumulation of drug-resistant mutations and significant side effects, however, thwart the efficacy of protease inhibitors for prolonged use and necessitate the design of new drugs with better properties.[3,5−7]

HIV-1 PR catalyzes cleavage of peptide bonds at specific sites in the viral Gag and Gag-Pol polyproteins during the maturation stage of the HIV-1 replication cycle.[8] The PR catalytic mechanism has been studied in depth since the first structures appeared in the literature.[9−11] HIV-1 PR belongs to the class of aspartic proteases, and utilizes two co-located aspartic acid residues to mediate peptide bond hydrolysis through an acid-base catalytic mechanism.[12] The active enzyme is a homodimer of two 99-amino acid subunits, each contributing a catalytic aspartate (Asp25 and Asp25′) to form the active site.[13] Solution enzyme kinetics and NMR measurements have established important mechanistic details of the PR catalysis:[14−19] (1) the two catalytic aspartates have very different pK_a values of ∼3.5 ± 0.1 and ∼6.0 ± 0.5, indicating that the catalytic site is monoprotonated; (2) the lytic water activated by the catalytic Asp residues is required for the hydrolysis reaction; (3) a kinetically competent amide hydrate tetrahedral intermediate is formed along the reaction

Received: February 25, 2020
Accepted: April 30, 2020
Published: May 14, 2020

https://dx.doi.org/10.1021/acsomega.0c00835
ACS Omega 2020, 5, 11605−11617

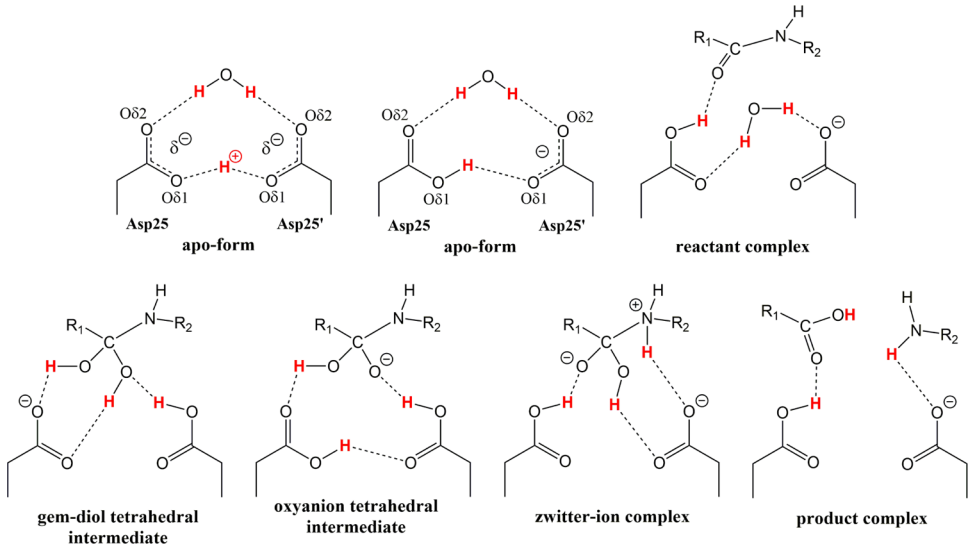

Figure 1. Chemical diagrams of several possible HIV-1 PR catalytic site structures in the mechanism of peptide bond hydrolysis. H atoms involved in the reaction are colored red, possible hydrogen bond interactions are shown as dashed lines. Catalytic site of the substrate-free (and inhibitor-free) form of enzyme is drawn containing a low-barrier hydrogen bond formed between Oδ1 oxygen atoms of the Asp dyad and with H covalently bound to Asp25 Oδ1. Many other arrangements for the H atom positions in the substrate-free form, reactant and tetrahedral intermediate complexes are also possible.

pathway, and (4) the tetrahedral intermediate collapses to the products in a rate-limiting step that involves proton transfer from a catalytic Asp to the nitrogen of the scissile C−N bond. However, atomic details of the PR catalytic mechanism are still being debated and proximity of multiple oxygen atoms in the catalytic site of PR indicates a possibility of multicenter (low-barrier) hydrogen bonds.[16,20−22] Throughout the reaction pathway, three hydrogen (H) atoms within the catalytic site are key players in peptide hydrolysis—two Hs originate on the lytic water and one H on the Asp residues before a substrate binds (Figure 1). In the tetrahedral intermediate, these H atoms are distributed among six oxygen atoms and over a hundred different combinations (or isomers) can be envisioned. Importantly, the orientation of the lytic water and the exact positions of Hs on the carboxylic side chains of Asp25 and Asp25′ in the reactant (Michaelis) complex, and the tetrahedral intermediate and product structures are not known. Lack of this information has led to a multitude of proposals for the PR catalytic mechanism based on theoretical calculations, NMR measurements, and X-ray crystallography.

In principle, the peptide bond hydrolysis reaction can proceed through a *gem*-diol tetrahedral intermediate, an oxyanion tetrahedral intermediate (Figure 1), or by a concerted mechanism with no stable intermediates along the reaction pathway.[13] Several earlier molecular modeling studies focused on the PR catalytic mechanism that includes a *gem*-diol tetrahedral intermediate.[23−26] Surprisingly, in these calculations the *gem*-diol tetrahedral intermediate was found to be either significantly more (−7 kcal/mol) or less (+12 kcal/mol) stable than the reactants, indicating that chosen models and/or levels of theory were inadequate. Other theoretical studies[27,28] demonstrated that the reaction could also proceed through a high-energy oxyanion tetrahedral intermediate (+14−18 kcal/mol relative to reactants), in which both Asp25 and Asp25′ were protonated. In this case, proton tunneling for the protonation of the tetrahedral intermediate nitrogen by a catalytic Asp was proposed to accomplish the rate acceleration,[16] in accordance with the inverse primary ^{15}N kinetic isotope effect.[19] More recent theoretical calculations considered many possible mechanisms and optimized structures of all 120 possible tetrahedral intermediates using density functional (DFT) and molecular orbital theories.[29−34] For example, cluster QM calculations by Garrec *et al.*[29] revealed a *gem*-diol tetrahedral intermediate having an energy of +3.4−4.8 kcal/mol relative to the reactants, whereas the only stable oxyanion tetrahedral intermediate was found to be greatly destabilized (+40 kcal/mol). On the other hand, QM/MM calculations of Krzeminska *et al.*[31] resulted in a much more stable oxyanion tetrahedral intermediate (+8 kcal/mol) that could readily overcome a 2 kcal/mol energy barrier to convert into the *gem*-diol tetrahedral intermediate, which was more stable than the reactants by −3 kcal/mol. These calculations also demonstrated that a metastable zwitterion intermediate on the path from the oxyanion to the products could exist (Figure 1), whereas the concerted mechanism with a cyclic transition state would require overcoming a very large, 43.5 kcal/mol, energy barrier. In the most recent study, however, Lawal *et al.*[34] revisited the concerted mechanism and showed that the pathway involving an acyclic transition state was feasible. Previous molecular modeling studies suggest that theoretical reaction energy barriers for the many modeled reaction pathways of the catalytic mechanism are in good agreement (based on the Eyring−Polanyi equation) with the corresponding experimental k_{cat} values of ∼1−5 s^{-1} for substrate hydrolysis by PR[14−19] at room temperature (RT), even though their specific atomic details are markedly different. Consequently, many different reaction pathways fit experimental measurements equally well, thus dissuading researchers from unequivocally determining the actual HIV-1 PR catalytic mechanism. In addition, based on the theoretically optimized *gem*-diol tetrahedral intermediate structures, one can hypothesize that a protease inhibitor containing the *gem*-diol chemical moiety with two hydroxyl groups should bind tighter to PR compared to the same inhibitor that has the commonly used hydroxyethylene isostere with one hydroxyl group, because the *gem*-diol moiety is capable of making an extra hydrogen bond

https://dx.doi.org/10.1021/acsomega.0c00835
ACS Omega 2020, 5, 11605−11617

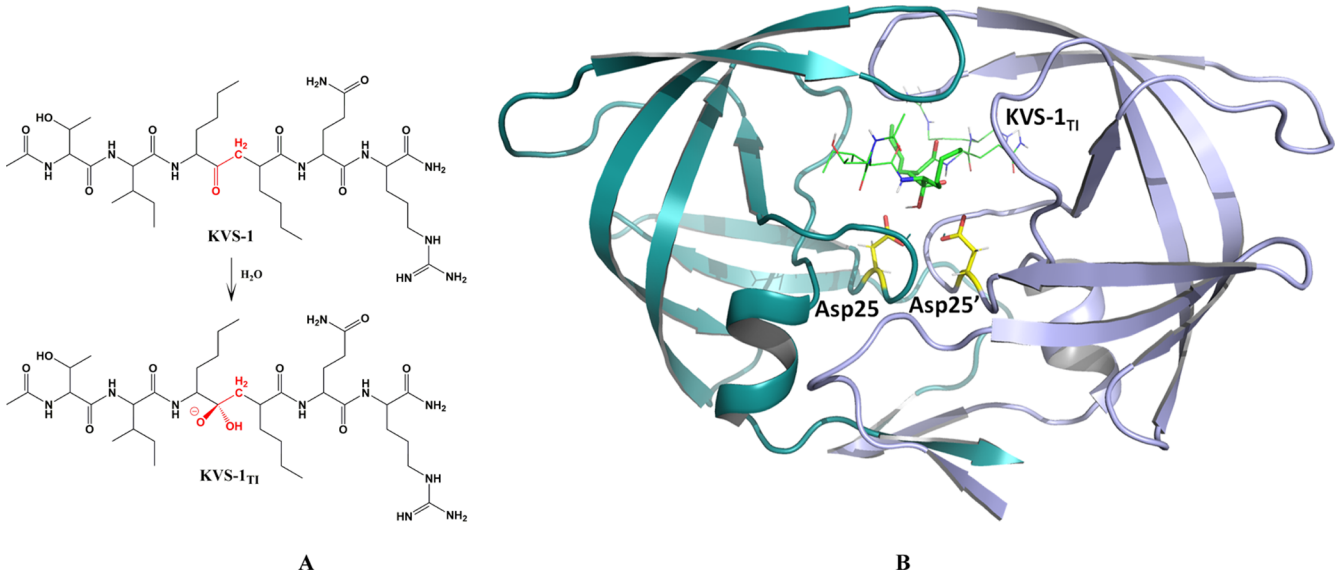

Figure 2. (A) Chemical diagram of the non-hydrolyzable hexapeptide KVS-1 and the resulting tetrahedral intermediate KVS-1_{TI}. The reactive ketomethylene isostere in KVS-1 and the tetrahedral intermediate moiety in KVS-1_{TI} are colored red. (B) Neutron structure of HIV-1 PR in complex with the oxyanion KVS-1_{TI} (green sticks). The catalytic Asp25 and Asp25′ are shown as yellow sticks. D atoms on Asp25, Asp25′, and KVS-1_{TI} are shown; nonexchangeable H atoms of KVS-1_{TI} are omitted for clarity.

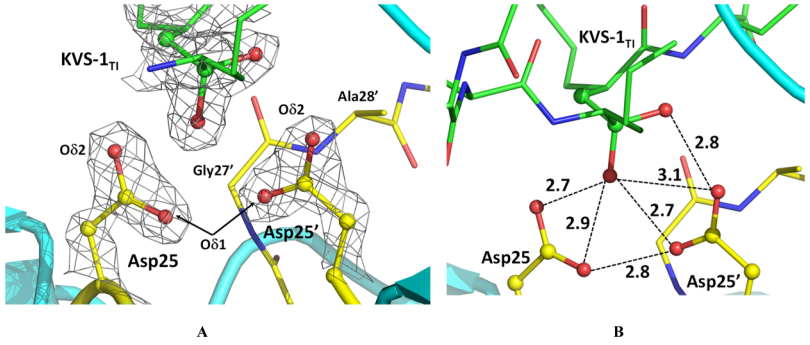

Figure 3. Catalytic site in the HIV-1 PR/KVS-1_{TI} complex. (A) $2F_O$-F_C electron density map contoured at the 2.5 σ level. Oxygen atoms of the Asp25 and Asp25′ carboxylic groups are labeled as Oδ1 and Oδ2 (B) possible hydrogen bonding interactions between the catalytic Asp dyad and the oxygen atoms of the tetrahedral intermediate. O···O distances are given in Å. Only X-ray diffraction data were used to generate the figure; thus, H and D atoms are omitted to demonstrate that noncovalent interactions cannot be reliably interpreted when locations of H atoms are unknown.

with the catalytic Asp dyad. In the current study, we make an attempt to directly address these two crucial points pertaining to the PR catalysis and drug design.

X-ray crystallography has been a method of choice in structural biology to obtain accurate three-dimensional structures of biomacromolecules and to link structure to function. A limited number of HIV-1 PR crystal structures in complex with tetrahedral intermediates have been reported, which, nonetheless, indicated that such intermediates can be trapped in the crystal lattice.[35−39] It was shown, initially, that nonhydrolyzable tetrahedral intermediates could be generated in the PR active site by a reaction with the lytic water attacking a pseudo-substrate where the amide nitrogen of the scissile peptide bond was replaced with a $-CF_2-$ or a keto group.[35,36] Also, in certain cases, the reactive, amide hydrate, tetrahedral intermediates could be trapped and their structures solved.[37−39] Nevertheless, positions of H atoms could not be resolved in these X-ray structures, leaving a significant gap in our understanding of the HIV-1 PR catalysis. The technique capable of accurately determining H atom positions and vizualizing hydrogen bonding in protein structures is neutron crystallography.[40,41] It permits detection of H (and its heavy isotope deuterium, D) atom locations and, hence, direct determination of the protonation states. Moreover, cold neutrons with wavelengths of ∼2−5 Å used in neutron crystallographic experiments cause no radiation damage to protein crystals so that the diffraction data can be collected under near-physiological conditions (usually at RT), eliminating the need to freeze crystals and to use cryo-protectant chemicals. However, the neutron diffraction data are normally weaker and less complete than the X-ray data. Combination of the X-ray and neutron diffraction data in a joint X-ray/neutron (XN) refinement provides an increased data-to-parameter ratio to produce complete protein structures containing accurate positions of all atoms, where heavy atom positions are mainly defined by the X-ray data and D atom positions are defined by the neutron data.[42]

We present here novel atomic details pertinent to the hydrolysis reaction catalyzed by HIV-1 PR. We determined a RT joint XN structure of HIV-1 PR in complex with the nonhydrolyzable ketomethylene hexapeptide inhibitor KVS-1, which is converted *in situ* into a tetrahedral intermediate

https://dx.doi.org/10.1021/acsomega.0c00835
ACS Omega 2020, 5, 11605−11617

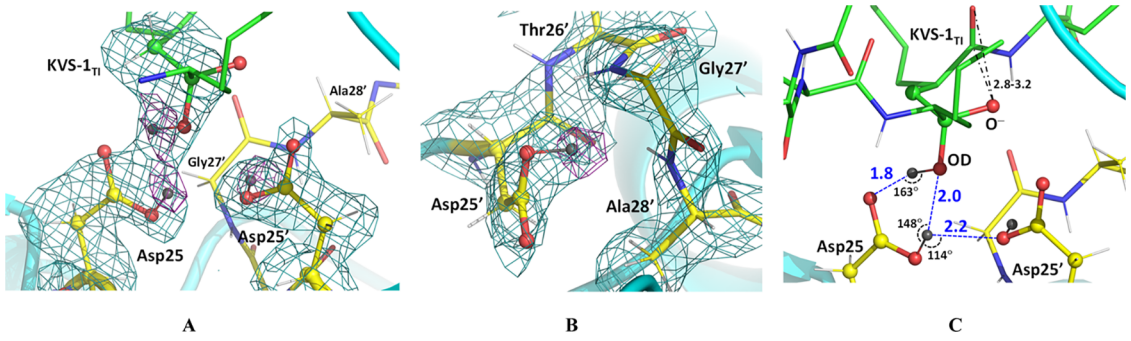

Figure 4. (A) The catalytic site of the HIV-1 PR/KVS-1_{TI} complex. (B) Catalytic Asp25′, and residues Thr26′, Gly27′, and Ala28′ making a small hydrophobic pocket where D bonded to the Asp25′ carboxylic group is facing. (C) Hydrogen bonds (blue dashed lines with O···D distances in Å, and O-D···O angles in deg.) made between the catalytic Asp dyad and the oxygen atoms of the intermediate. The negatively charged oxygen atom of the oxyanion makes close 2.8−3.2 Å contacts with next carbonyl in the hexapeptide main chain. For panels A and B, $2F_O$-F_C neutron scattering length density map at a 2.2 Å resolution is contoured at the 1.5 σ level; the F_O-F_C-omit difference neutron scattering length density map is the violet mesh contoured at the 3 σ level, indicating the locations of the three D atoms (dark gray spheres) involved in catalysis (other D atoms are light gray). H atoms of KVS-1_{TI} are omitted for clarity.

analogue (KVS-1_{TI})[43,44] (Figures 2 and 3). We observed both catalytic Asp residues protonated on their Oδ1 oxygen atoms (labelled in Figure 3 and consistently referred to throughout the manuscript), and one protonated and one deprotonated oxygen on KVS-1_{TI}. This rather unexpected result implies that the trapped tetrahedral intermediate moiety is an oxyanion, rather than the *gem*-diol. We support our experimental findings with cluster QM and QM/MM calculations. We also obtained a RT X-ray structure of HIV-1 PR in complex with keto-darunavir (keto-DRV), in which the hydroxyethylene isostere of the clinical inhibitor darunavir (DRV) was oxidized into the ketomethylene moiety. Similar to our joint XN structure, the ketomethylene of keto-DRV was converted to a tetrahedral intermediate analogue to give DRV_{TI} bound in the PR active site cavity. The extent of inhibition of PR by keto-DRV was assessed using isothermal titration calorimetry (ITC).

RESULTS

Neutrons Reveal Hydrated KVS-1 is a Tetrahedral Oxyanion Bound to HIV-1 PR. To obtain the complex with KVS-1_{TI} we chose an HIV-1 PR triple mutant variant (PR_{TM}), which contains three substitutions V32I, I47V, and V82I associated with drug resistance (Table S1), because of its demonstrated success to afford neutron diffraction quality crystals and because the resistance mutations do not introduce considerable distortions in ligand binding compared to the wild-type enzyme.[45,46] We collected RT neutron crystallographic data to 2.2 Å resolution from a very small crystal of ~0.15 mm^3 in volume. The neutron data were refined jointly with a 1.85 Å resolution RT X-ray dataset to give the joint XN structure of the PR_{TM}/KVS-1_{TI} complex. The electron density maps calculated from the X-ray data (Figures 3A, and S1) clearly show that the central carbon atom is sp^3 hybridized, confirming that the ketomethylene moiety of KVS-1 has reacted with a water molecule to give a formal tetrahedral intermediate with two oxygen atoms bound to the central carbon, in agreement with the previous low-temperature X-ray structures of HIV-1 PR in complex with this modified hexapeptide.[43,44] The electron density for KVS-1_{TI} is strong and well defined (Figure S1); thus, we saw no indication of the KVS-1_{TI} static disorder in the PR_{TM}/KVS-1_{TI} complex, which was previously observed in many PR-ligand structures where the ligand can have two orientations related by a 180° rotation with similar occupancies because of the 2-fold symmetry of the PR dimer. Such static disorder has not been found in our joint XN structures of the deuterated HIV-1 PR.[45,46] Examination of the O···O distances between the oxygen atoms of the tetrahedral intermediate moiety and the carboxylic groups of the Asp dyad reveals a possibility of six hydrogen bonds with the distances in the range of 2.7−3.1 Å (Figure 3B). Correct assignment of the hydrogen bonds, however, cannot be made based on the X-ray data, because H atom locations are not seen. Conversely, D atoms are visible within the catalytic site of the PR_{TM}/KVS-1_{TI} complex in the neutron scattering length density maps (also referred to as nuclear density maps) (Figures 4A and S2A); however, for simplicity, we use the standard chemical conventions such as protonation states and hydrogen bonds. There is a clear density identifying three D atoms—one each on Asp25, Asp25′, and a hydroxyl of the tetrahedral intermediate moiety (Figure 4A,B). Therefore, according to our joint XN structure, the carboxylic groups of the catalytic Asp dyad are both protonated on their Oδ1 atoms, and, thus, have neutral charges. However, within the tetrahedral intermediate moiety, one oxygen is protonated, whereas the other is not, hence having a −1 charge. This observation unequivocally leads us to conclude that the tetrahedral intermediate moiety is an oxyanion, rather than the *gem*-diol. Importantly, the Asp25 O-D bond is in the carboxylic group plane and is directed toward the protonated tetrahedral intermediate hydroxyl and the Asp25′ side chain, forming a bifurcated hydrogen bond (Figure 4C). However, the Asp25′ O-D bond is rotated away from both Asp25 and the protonated tetrahedral intermediate hydroxyl by almost 90° into a small hydrophobic cavity formed by the Thr26′-Gly27′-Ala28′ turn so that it makes no hydrogen bonding interactions (Figures 4B and S2B). The protonated tetrahedral intermediate hydroxyl group also makes a hydrogen bond with the Oδ2 atom of Asp25. This hydrogen bonding analysis demonstrates that only three out of six possible hydrogen bonds form within the tetrahedral intermediate moiety and the catalytic Asp dyad. The catalytic water molecule in the unliganded HIV-1 PR structure (PDB code 1LV1) lies within 0.7 Å from the protonated tetrahedral intermediate hydroxyl of KVS-1_{TI} complexed to PR_{TM} (Figure S3A). Based on these observations, we can now deduce that the protonated tetrahedral intermediate hydroxyl comes from the lytic water

https://dx.doi.org/10.1021/acsomega.0c00835
ACS Omega 2020, 5, 11605−11617

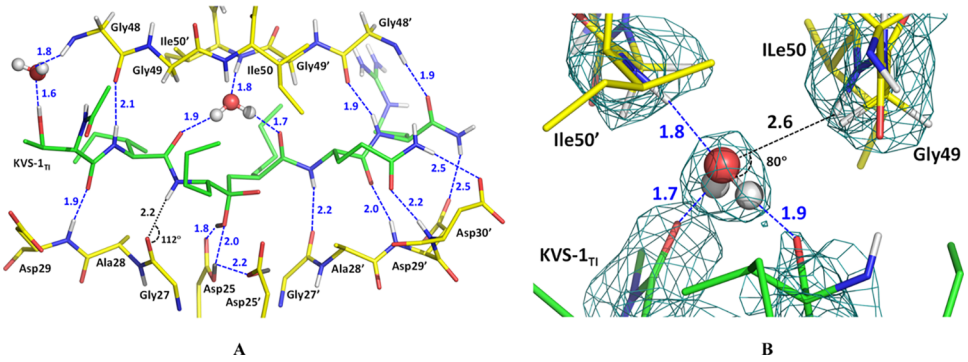

Figure 5. (A) Hydrogen bonding and water-mediated interactions, shown as blue-dashed lines connecting O or N atoms with D atoms (O···D and N···D), between KVS-1_{TI} and the active site residues in PR_{TM}. The N−D···O contact with Gly27 main chain carbonyl is significantly distorted from the ideal hydrogen bond geometry, with the N−D vector being almost perpendicular to the carbonyl plane. (B) Water-mediated interactions with main chain amides of Ile50 and Ile50′. The flap water makes a hydrogen bond with the main chain amide of Ile50′, but not with Ile50 because the O···D distance of 2.6 Å is too long.

molecule and the oxyanion oxygen is from the ketomethylene carbonyl group of KVS-1. Furthermore, the D atom connected to Asp25 is the original proton present within the PR catalytic site before the substrate binds, whereas the D atoms on tetrahedral intermediate hydroxyl and Asp25′ come from the lytic water molecule.

KVS-1_{TI} makes seven additional moderate hydrogen bonds with the main chain amide nitrogens of Asp29, Asp29′, Asp30′, and Gly48′, and with the main chain carbonyls of Gly48, Gly27′, and Gly48′ (Figure 5A), with D···O distances of 1.9−2.2 Å, and two weaker hydrogen bonds with Asp29′ and Asp30′ side chain carboxylates. It also interacts with the Gly48 main chain amide nitrogen through a water-mediated contact. The other water-mediated interaction connecting two carbonyl groups of KVS-1_{TI} with the main chain amides of Ile50 and Ile50′ flap residues is rather peculiar (Figures 5B and S4). The flap D_2O water molecule has such an orientation that it forms three hydrogen bonds instead of possible four. The flap D_2O donates both D atoms to hydrogen bond with two carbonyls of KVS-1_{TI} and accepts a main chain amide D to form a hydrogen bond with Ile50′. The main chain amide of Ile50 is also capable of participating in a hydrogen bond with the flap water, but the D···O distance is elongated (2.6 Å) and the amide makes an acute angle of 80° with the D_2O plane. The geometry of this contact is, therefore, far outside the normal parameters for a hydrogen bond[47] and this flap is anchored more weakly to the PR active site. Such an unexpected hydrogen bonding network around the flap water molecule has been observed previously in our joint XN structures of wild-type PR and PR_{TM} in complex with clinical drugs amprenavir and DRV[45,46] and agrees with the assessment based on NMR measurements[44] that found one PR flap more dynamic than the other.

It is instructive to compare the binding of the hydrated KVS-1_{TI} in the PR_{TM} active site cavity to that of the actual amide hydrate tetrahedral intermediates published previously.[37−39] Among the four amide hydrate tetrahedral intermediate structures determined at 100 K, three correspond to complexes with the wild type PR (PDB IDs 3B7V, 4FL8, and 5YRS), with two, 4FL8 and 5YRS, having the tetrahedral intermediate peptides disordered over two orientations related by a 180° flip, with 50% occupancy each, and 3B7V having the peptide in one orientation with 60% occupancy. The fourth structure (PDB ID 3B80) is of PR I54V mutant variant in which the tetrahedral intermediate has one orientation with 60% occupancy. Importantly, the electron density for the peptidic ligand is stronger in the 3B7V structure. Although all the complexes superimpose well, with the root mean square deviation (rmsd) on the main chain atoms of 0.2−0.4 Å, the tetrahedral intermediate moiety in the PR_{I54V}-tetrahedral intermediate complex aligns best with that of our joint XN structure of PR_{TM}/KVS-1_{TI} (Figure S3B); however, its electron density is rather weak. All non-covalent O···O distances within the PR_{I54V} catalytic site, except for one, are virtually the same compared to those in PR_{TM}/KVS-1_{TI}. In our XN structure, one O···O distance of 2.8 Å is longer than the equivalent one of 2.5 Å in the PR_{I54V} mutant TI complex, and it corresponds to an interaction between the oxyanion oxygen and the Oδ2 of Asp25′. In the PR_{WT}/tetrahedral intermediate structure 3B7V, this distance was found to be even shorter, at 2.3 Å, implying protonation of one of the oxygens and suggesting formation of a strong ionic hydrogen bond (Figure S3C). We would like to emphasize here that hydrogen atoms have not been observed in these low temperature X-ray structures, therefore, the accurate assignment of hydrogen bonds cannot be made.

Low Temperature Narrows the PR_{TM} Substrate-Binding Channel. To find out if temperature has an effect on the structure of the PR_{TM}/KVS-1_{TI} complex, we obtained its X-ray structure at 100 K at 1.31 Å resolution. Overall, the room-temperature joint XN structure and the low-temperature X-ray structure superimpose well, with the rmsd on the main chain atoms of 0.3 Å and with the rmsd of 0.1 Å for all atoms of KVS-1_{TI}. Closer examination of the PR_{TM} substrate binding channel, however, reveals more significant differences in the relative positions of residues in the two structures. Many residues in the PR_{TM} active site (substrate binding channel) have shifted by 0.3−0.4 Å toward KVS-1_{TI}, reducing the distances across the substrate binding channel by at least 0.5−0.6 Å. The most dramatic shift is observed for the 80's loops in PR_{TM}, containing residues Thr80−Pro81−Ile82 and Thr80′−Pro81′−Ile82′ that are part of the active site (Figure S5). The distance between Pro81 and Pro81′ decreases by ∼1 Å in the low temperature structure, which is a significant change based on the estimated coordinate errors for the two structures of 0.05 Å (100 K X-ray structure) and 0.14 Å (room-temperature joint XN structure). Considering the shape of the PR_{TM} substrate-binding channel as a cylinder and taking into account the shifts in residue positions between the room- and low-temperature structures, we estimate that at 100 K the active

https://dx.doi.org/10.1021/acsomega.0c00835
ACS Omega 2020, 5, 11605−11617

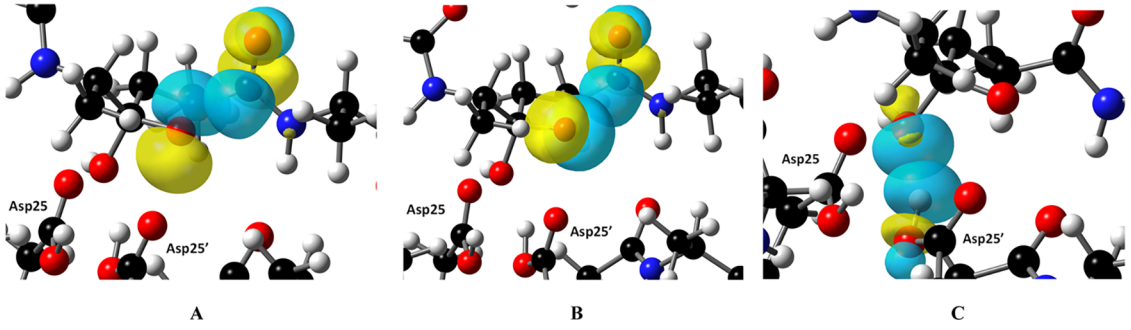

Figure 6. Orbital interactions in the protease catalytic site. (A,B) Two n → π^* interactions occur within KVS-1_{TI} between two lone electron pairs of the negatively charged oxygen and an antibonding π^* orbital of the nearby carbonyl group. (C) An n → σ^* interaction between the protonated tetrahedral intermediate hydroxyl and Asp25′ hydroxyl, signifying a strong hydrogen bond formation.

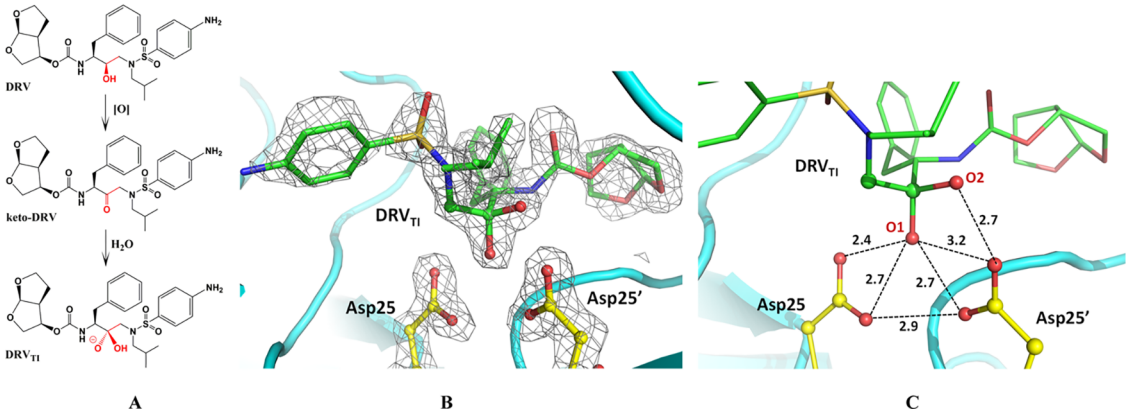

Figure 7. (A) Chemical diagram of clinical inhibitor DRV, its oxidized analogue keto-DRV, and the resulting tetrahedral intermediate DRV_{TI}. DRV_{TI} is shown as an oxyanion assuming its protonation state is the same as for KVS-1_{TI}. (B) Catalytic site of the PR_{TM}/DRV_{TI} complex showing the $2F_O$-F_C electron density map contoured at the 2.0 σ level. (C) Possible hydrogen bonding interactions between the Asp dyad and the tetrahedral intermediate moiety of DRV_{TI} are based on the O···O distances given in Å.

site volume has shrunk by ∼20−30 Å^3 compared to its size at RT, which also leads to apparent shorter hydrophobic interactions between KVS-1_{TI} and the side chains of the PR_{TM} residues. Interestingly, the side chain conformations have mostly remained the same in the two structures unlike in the PR_{TM}/APV structures reported previously,[45] except for Ile82 whose two alternate conformations visible at low temperature are different from the single conformation observed in the RT joint XN structure.

Oxyanion Charge is Delocalized by Hyperconjugation, but KVS-1_{TI} is Unstable. How is the formal negative charge of −1 on the oxyanion tetrahedral intermediate oxygen of KVS-1_{TI} stabilized in the PR_{TM}/KVS-1_{TI} complex used to determine its structure? To understand how such stabilization can be achieved, we performed cluster QM calculations on a 194-atom model built using atomic coordinates from our joint XN structure (D atoms were replaced with H atoms) and performed NBO analysis of the model to estimate the strength of noncovalent interactions. The distance of 2.8−3.2 Å between the negatively charged oxygen of the tetrahedral intermediate and the carbonyl group of the next peptide bond (Figure 4C) suggests a possibility of charge delocalization by means of an n → π^* charge transfer interaction, that is through-space hyperconjugation. Indeed, according to our NBO analysis, two such interactions of the charged tetrahedral intermediate oxygen lone pairs with an antibonding π^* orbital of the carbonyl are present, with the energies of 1.92 and 0.67 kcal/mol, indicating a strong charge delocalization onto the carbonyl π system (Figure 6A,B). It is evident that the n → π^* interactions occurring within the oxyanion tetrahedral intermediate should have a significant stabilization effect. These n → π^* interactions are possibly enhanced by a strong repulsive electrostatic interaction with the Asp25′ carboxylic Oδ2 oxygen positioned 2.8 Å away from the negatively charged tetrahedral intermediate oxygen. The O···O repulsion, which is unfavorable for the oxyanion stability, however, may still dominate over the hypercojugation, as discussed below. We then shifted the H atom from Asp25′ carboxyl to the deprotonated oxygen of the tetrahedral intermediate to create a *gem*-diol, optimized its geometry, and performed NBO analysis. In our *gem*-diol tetrahedral intermediate Asp25′ Oδ2 now makes a hydrogen bond with the new hydroxyl group of the tetrahedral intermediate, instead of the repulsive interaction with the oxyanion. There is only one n → π^* interaction of 1.52 kcal/mol with the carbonyl group of the next peptide bond in the *gem*-diol tetrahedral intermediate, in agreement with the previously computed *gem*-diol tetrahedral intermediate that had a different juxtaposition of H atoms.[48] This interaction energy in our *gem*-diol tetrahedral intermediate is weaker, as expected, than in our oxyanion tetrahedral intermediate.

To shed light on the Asp25′ Oδ1-H bond rotation away from the tetrahedral intermediate moiety hydroxyl of KVS-1_{TI}, we examined the interaction of these two chemical groups. Our cluster QM calculation optimizes the H atom of the Asp25′ Oδ1-H to be in plane with the carboxylic group, resulting in a

https://dx.doi.org/10.1021/acsomega.0c00835
ACS Omega 2020, 5, 11605−11617

strong hydrogen bond with the protonated hydroxyl of the tetrahedral intermediate. The strength of this hydrogen bond can be measured by the charge transfer from a tetrahedral intermediate hydroxyl lone pair to the σ^* orbital of the Asp25′ Oδ1-H bond (Figure 6C). NBO analysis reveals that this n → σ^* interaction is 26 kcal/mol. By comparison, the n → σ^* interactions of the two tetrahedral intermediate hydroxyl lone pairs with the Asp25 Oδ1-H bond are an order of magnitude weaker at 2.2 and 2.8 kcal/mol. When Asp25′ Oδ1-H was fixed in the geometry observed in the joint XN structure, the n → σ^* interaction was reduced to just 0.1 kcal/mol, indicating that the charge transfer component of the hydrogen bond was essentially abolished.

We then optimized the geometry of the PR_{TM}/KVS-1_{TI} complex starting from the joint XN structure atomic coordinates using the QM/MM methodology. Unexpectedly, the strong hydrogen bond of Asp25 Oδ1-H with the protonated hydroxyl of the tetrahedral intermediate leads to a spontaneous proton transfer to the tetrahedral intermediate oxygen and the generated water molecule's cleavage off the tetrahedral intermediate moiety. The tetrahedral intermediate carbon atom is rehybridized from sp^3 to sp^2 producing a ketone group. Therefore, both reactants, KVS-1 containing the initial ketomethylene isostere and the lytic water molecule, are regenerated during the QM/MM geometry optimization (Figure S6). This implies that the PR_{TM}/KVS-1_{TI} complex is metastable with the overall energy higher than that of the reactants.

Keto-DRV Binds to HIV-1 PR_{TM} to Give a Tetrahedral Intermediate Complex. The clinical inhibitor DRV contains the hydroxyethylene isostere whose hydroxy group forms a hydrogen bond tightly with the catalytic Asp dyad.[46] We oxidized this hydroxyl to give the ketomethylene isostere, as in KVS-1, thus producing keto-DRV (Figure 7A). Keto-DRV was co-crystallized with PR_{TM} and a RT X-ray structure of the complex was obtained at 1.80 Å resolution. In the electron density map, we clearly observed that keto-DRV was converted to DRV_{TI} bound to the catalytic Asp dyad, having the sp^3-hybridized tetrahedral carbon connected to two oxygens (Figure 7B) similar to the structure and binding mode of KVS-1_{TI}. One oxygen (O1 on Figure 7C) has an O···O contact of 2.4 Å with Asp25 Oδ2, which is somewhat shorter than that made by KVS-1_{TI}. O1 of DRV_{TI} is presumably protonated as in KVS-1_{TI} and thus makes a strong hydrogen bond with Asp25, whereas all other distances to the Asp dyad carboxylic oxygens are very similar to those in the PR_{TM}/KVS-1_{TI} complex. As in PR_{TM}/KVS-1_{TI}, the second oxygen of DRV_{TI} (O2 on Figure 7C) is 2.7 Å away from Asp25′ Oδ2 and, by analogy with the joint XN structure of PR_{TM}/KVS-1_{TI} is probably an oxyanion. We also superimposed our PR_{TM}/DRV_{TI} structure on the previously published neutron structure of the PR_{TM}/DRV complex obtained at pH 6.[46] The two structures aligned remarkably well, with the rmsd on main chain atoms of less than 0.1 Å. DRV and DRV_{TI} essentially occupy identical positions in the PR_{TM} active site channels (Figure S7). Their two matching oxygen atoms have virtually identical contacts with the Asp dyad. The only difference between the ligands is the presence of an extra oxygen in DRV_{TI}. In PR_{TM}/DRV, the drug's hydroxy group participates in an unusual low-barrier hydrogen bond, with the Asp25′ D atom being equidistant to three oxygen atoms and donates its D to form a bifurcated hydrogen bond with Asp25 Oδ1 and Oδ2. We anticipate that the distribution of H atoms in PR_{TM}/DRV_{TI} would be identical to their locations in the joint XN structure of PR_{TM}/KVS-1_{TI}.

ITC Provides Evidence that Keto-DRV is Inferior to DRV. Because our QM/MM calculations on the PR_{TM}/KVS-1_{TI} complex demonstrated instability of the oxyanion tetrahedral intermediate, we reasoned that keto-DRV might be a weaker inhibitor of the HIV-1 PR than DRV, if the DRV_{TI} we observed in the RT X-ray structure of PR_{TM}/DRV_{TI} is also an oxyanion. Therefore, we performed ITC and enzyme inhibition measurements using wild-type PR (PR_{WT}), PR_{TM}, and a clinical drug resistant variant PR20 with DRV and keto-DRV. From Table 1 and Figures 8 (and S8), it is apparent that

Table 1. Comparison of the Binding Affinity of DRV and Keto-DRV to PR_{WT}, PR_{TM}, and PR20

	K_d, nM PR_{WT}	K_d, nM PR_{TM}	K_d, nM PR20
DRV	0.005[72]	11 ± 6.5	62 ± 7
keto-DRV	79 ± 8.3	710 ± 240	nd[a]

[a]Not determined because of very weak binding ($K_d \gg 10\ \mu M$).

the binding affinity of keto-DRV to the three PR variants is 2−4 orders of magnitude weaker than that of DRV, indicating that the formed PR/DRV_{TI} complexes are markedly less stable than the corresponding PR/DRV complexes. Moreover, affinity of keto-DRV to PR20 could not be determined with ITC, which is in agreement with our failed attempts to grow crystals of this complex. We then determined how well keto-DRV inhibits PR-catalyzed hydrolysis of a substrate (Figures 8 and S9). The initial rates and activity plots of substrate hydrolysis by PR_{WT}, PR_{TM}, and PR20 clearly indicate that keto-DRV is a weaker inhibitor than DRV. To slow the enzyme activity below 20% of the initial values (i.e., when no inhibitor was present) requires 1:2 and 1:20 enzyme-to-keto-DRV molar ratio for PR_{WT} and PR_{TM}, respectively, whereas PR20 is not inhibited at all even at a 1:20 molar ratio. In contrast, DRV already fully inhibits PR_{TM} at a 1:1 molar ratio at these concentrations.

DISCUSSION

HIV-1 PR is an indispensable viral enzyme that drives the maturation stage of the HIV-1 lifecycle ensuring conversion of immature viral particles into infectious virions. Thus, PR has been considered a crucial target for the design and development of anti-HIV drugs, and its structure and function have been thoroughly studied.[5,12] As a member of the aspartic protease family of enzymes, HIV-1 PR catalyzes peptide bond cleavage by utilizing a pair of co-located Asp residues, one of which is protonated, and a lytic water molecule that is symmetrically hydrogen bonded to the catalytic Asp dyad in the substrate-free (or inhibitor-free) form of the enzyme.[13,16] The juxtaposition and interplay of the three H atoms present in the catalytic site of HIV-1 PR throughout the peptide bond hydrolysis reaction determines the actual chemical mechanism of amide bond hydrolysis. Although many reaction pathways have been considered using theoretical calculations,[23,24] there is no experimental evidence on the exact location and movement of these H atoms within the PR catalytic site along the reaction coordinate because protons are normally not seen in X-ray structures. Consequently, an important unanswered mechanistic question remains: does the peptide bond hydrolysis reaction catalyzed by the HIV-1 PR proceed through a stable *gem*-diol intermediate, a metastable oxyanion intermediate, or possibly an oxyanion transition state? The

https://dx.doi.org/10.1021/acsomega.0c00835
ACS Omega 2020, 5, 11605−11617

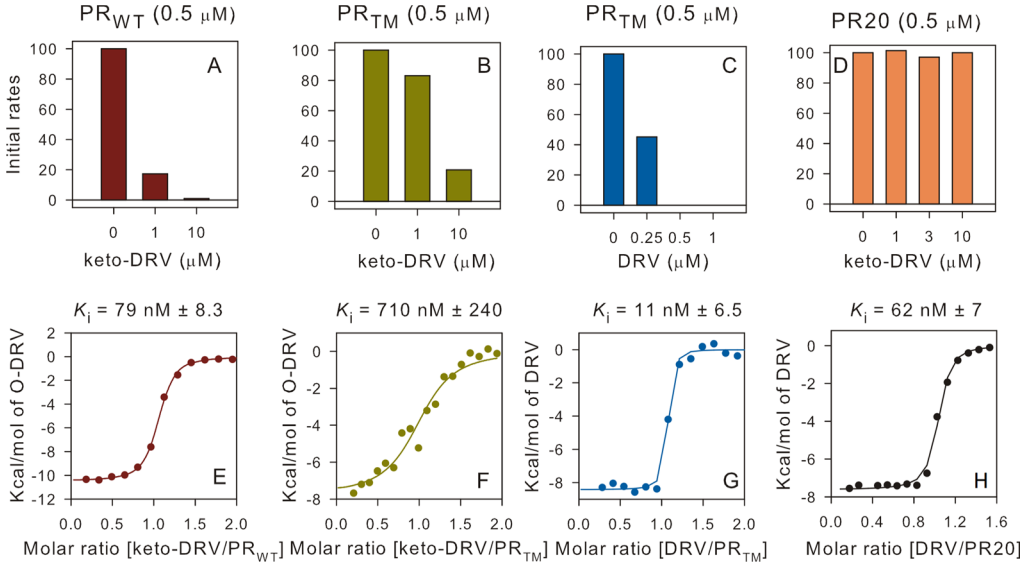

Figure 8. Initial rates for the hydrolysis of the chromogenic substrate catalyzed by the mature PR variants (panels A–D) and binding isotherms for complex formation of keto-DRV with PR_{WT} and PR_{TM} and DRV with PR_{TM} and PR20 (panels E–H).

latter case corresponds to a concerted mechanism with multiple possible pathways, each having no intermediates on the reaction potential energy surface.[13,31,34]

We approached this question by using neutron diffraction to probe the structure of a tetrahedral intermediate formed by the attack of the lytic water molecule on the carbonyl of the non-hydrolysable ketomethylene isostere of the hexapeptide KVS-1.[43,44] Neutrons allowed us to directly visualize H atoms (observed as D atoms) in the resulting PR_{TM}/KVS-1_{TI} complex at RT and accurately determine their exact locations. We observed protonation of only one hydroxy group of the tetrahedral intermediate moiety, whereas the other appears to be deprotonated. Thus, the tetrahedral intermediate moiety is an oxyanion, having an OH group and a negatively charged O^-, rather than a neutral *gem*-diol with two OH groups. Moreover, both Asp25 and Asp25′ were found to be protonated on the "inner" (Oδ1) atoms, so that the catalytic Asp dyad bears a neutral charge in the complex with a mimic of the anionic tetrahedral intermediate. The doubly protonated catalytic Asp dyad was previously considered in the HIV-1 PR catalytic mechanism calculations, with the reaction proceeding through a metastable oxyanion tetrahedral intermediate[16,27,28,31] or an oxyanion transition state,[34] where the two H atoms were either placed on both "outer" (Oδ2) Asp oxygens, or each positioned on the "inner" and "outer" oxygens. The two possible theoretical structures of the oxyanion tetrahedral intermediate with both Asp25 and Asp25′ protonated on the "inner" oxygens were optimized by Garrec *et al.*[29] using cluster DFT calculations. Both structures were found to be unstable during geometry optimizations, in agreement with our QM/MM calculations on the joint XN structure of PR_{TM}/KVS-1_{TI}.

Interestingly, our results would agree with the concerted acyclic reaction mechanism proposed very recently by Lawal *et al.*,[34] but would disagree with the NMR measurements of kinetic isotope effects done by Kipp *et al.*[17] that are consistent with the formation of a *gem*-diol intermediate, which falls apart into products after a proton is transferred from Asp25′ to the amine of the scissile C–N bond in the rate-limiting step. Also, in the previous X-ray structures containing trapped amide hydrate tetrahedral intermediates, one of the two tetrahedral intermediate hydroxyls made very short interactions of <2.5 Å with Asp25′, indicative of strong hydrogen bonding and protonation of either of the oxygens, whereas in PR_{TM}/KVS-1_{TI} the corresponding distance is 2.8 Å and both oxygens are deprotonated. Hence, we note that one should not ignore a possibility that such ketomethylene isostere-containing compounds may not be proper analogues of the tetrahedral intermediate formed in the HIV-1 PR catalyzed hydrolysis of substrates, and caution has to be exercised when using them in mechanistic enzymatic studies.

It is of note that PR_{TM}/KVS-1_{TI} and PR_{TM}/DRV_{TI} complexes containing oxyanion tetrahedral intermediate mimics can be trapped in crystals, and that the PR/KVS-1_{TI} structure could be previously studied in solution with NMR.[43,44] Solution inhibition studies by Marinier *et al.*[49] indicated that some peptides with the ketomethylene functionality showed a 10-fold increased inhibition of the PR as compared to those having the hydroxyethylene isostere. The fact that we were able to trap KVS-1_{TI} as oxyanion tetrahedral intermediate within the PR_{TM}/KVS-1_{TI} crystal lattice correlates well with these solution inhibition studies, even though our QM/MM calculations indicate geometry-optimized PR_{TM}/KVS-1_{TI} reverts to reactants. In the case of keto-DRV, the resulting DRV_{TI} is 2–4 orders of magnitude weaker inhibitor of PR than the unmodified clinical inhibitor DRV. Because the chemical modification of DRV to give keto-DRV only alters the central hydroxyl into a keto-group, the large differences in the binding affinity of DRV and keto-DRV (and by extension of DRV_{TI}) may be because of this modification and/or because of the repulsion of the negatively charged oxyanion and Asp25′ carboxylic oxygen. This inference appears to be in excellent agreement with the conclusion of Sayer *et al.*[50] stating that a major contribution to the binding affinities of PR inhibitors like DRV comes from specific hydrogen bonding interactions with the catalytic Asp dyad.

Based on our crystallographic and solution data, it is not unreasonable to suggest that if DRV_{TI} were a *gem*-diol, it would have been a superior inhibitor to DRV because the second OH group of the tetrahedral intermediate moiety would create an

https://dx.doi.org/10.1021/acsomega.0c00835
ACS Omega 2020, 5, 11605–11617

additional hydrogen-bonding capability compared to DRV. However, based on our results of weaker PR inhibition by keto-DRV compared to DRV, we estimate that nonpeptidic inhibitors, such as DRV, containing a carbonyl functional group that is converted to the geminal oxyanion, would be inferior to those with a single hydroxyl interacting with the catalytic Asp dyad, as was also demonstrated in the early studies of HIV-1 PR inhibitors having a vicinal di-ketone isostere.[35] Nevertheless, inhibitors containing two hydroxyl groups (or a hydroxyl and an amine group) in the vicinal configuration, potentially adding an extra hydrogen bond to the catalytic Asp residues, might be of interest for future drug design. Our results also highlight the importance of obtaining structural information at near physiological temperatures, especially for the drug-resistant protease complexes with clinical drugs, as was also documented by us previously.[45]

CONCLUSION

By using neutron diffraction, we visualized hydrogen atoms in an enzyme−substrate analogue complex. We demonstrate that the *in situ* generated tetrahedral hydrated form of the keto isostere of the KVS-1 peptide (KVS-1_{TI}) bound to the HIV-1 PR_{TM} is an oxyanion, with one oxygen atom protonated (OH) and the other deprotonated (O^-). Asp25 and Asp25′ were found to be both protonated, and the Asp25′ carboxylic O−H bond is rotated away from Asp25 and the tetrahedral intermediate moiety into a hydrophobic pocket lined up by residues Thr26′-Gly27′-Ala28′. The trapped oxyanion tetrahedral intermediate is stabilized by the oxyanion negative charge delocalization into the π system of the adjacent carbonyl group through strong n $\rightarrow$ π^* hyperconjugative interactions, even though it is unstable according to our QM/MM geometry optimizations. We also show that keto-DRV, similar to KVS-1, is capable of producing a tetrahedral intermediate DRV_{TI} when bound to HIV-1 PR. However, keto-DRV turned out to be a much weaker inhibitor than DRV. Finally, our observations indicate that novel protease inhibitors may benefit from functionalities capable of making additional hydrogen bonds with the catalytic Asp dyad.

MATERIALS AND METHODS

General Information. Protein purification supplies were purchased from GE Healthcare (Piscataway, New Jersey, USA). Crystallization reagents were purchased from Hampton Research (Aliso Viejo, California, USA). Synthesis of KVS-1 has been described previously.[43,44] DRV was obtained through the NIH AIDS reagent program. Keto-DRV was custom synthesized from DRV by Nanosyn (Santa Clara, CA).

Protein Expression, Purification, and Crystallization. The HIV-1 protease (pseudo-wild type) construct bears the stabilizing substitution mutations Q7K, L33I, L63I, C67A, and C95A to restrict autoproteolysis and cysteine-thiol oxidation.[51] The PR_{TM} has additional substitutions V32I, I47V, and V82I associated with drug resistance. Expression and purification from inclusion bodies of wild-type PR, PR_{TM}, and extremely drug-resistant clinical isolate PR20 (Table S1) using Luria−Bertani were performed in *Escherichia coli* (BL21-DE3) cells as described previously.[52−54] To obtain deuterated PR_{TM}, the minimal medium made with 99.8% D_2O and hydrogenous glycerol as the sole carbon source was used, and the deuterated enzyme was isolated, purified, and refolded from inclusion bodies in H_2O buffers using standard protocols.[55] KVS-1 stock solution [40 mM in dimethyl sulfoxide (DMSO)] was mixed with 3.0 mg/mL HIV-1 PR in a molar ratio of 10:1 for crystallization of the complex. For neutron crystallography, crystals were grown in 200 μL drops made by mixing the sample and the reservoir solution (0.1 M MES, 0.9 M NaCl, and pH 6.0) at a 1:1 ratio in a sitting drop setup using a Hampton Research sandwich box setup. A neutron-diffraction quality crystal grew to ~0.15 mm^3 in volume and the labile H atoms in the crystal were allowed to exchange with D by the D_2O vapor for several months before the neutron data collection. The crystal was mounted in a quartz capillary containing the reservoir solution made with 99.97% D_2O for the neutron diffraction data. Smaller crystals grown under the same reservoir conditions were used for X-ray data collection. Keto-DRV (20 mM stock in DMSO) was mixed with 3.0 mg/mL PR_{TM} in a molar ratio of 5:1. Crystals of the complex were grown in 300 μL drops made by mixing the sample and the reservoir solution (0.1 M MES, 1.0 M NaCl, pH 6.0 in H_2O) at a 1:1 ratio in the 9-well glass plate/sandwich box sitting drop setup.

X-ray and Neutron Data Collection. RT X-ray crystallographic data for PR_{TM}/KVS-1_{TI} and PR_{TM}/DRV_{TI} crystals were collected on a Rigaku HighFlux HomeLab instrument equipped with a MicroMax-007 HF X-ray generator and Osmic VariMax optics. The diffraction images were obtained using an R-Axis IV++ image plate detector. Diffraction data were integrated and scaled using the HKL3000 software suite indicating no appreciable radiation damage.[56] Low temperature 100 K crystallographic data for PR_{TM}/KVS-1_{TI} were collected on the 5.0.3 beamline at the Advanced Light Source, Lawrence Berkeley National Laboratory, USA, and the diffraction data were integrated and scaled using the *mosflm* from CCP4 software suite.[57] The preliminary neutron diffraction data at RT were collected on the IMAGINE[58] instrument located at the High Flux Isotope Reactor (Oak Ridge National Laboratory). The full quasi-Laue neutron diffraction dataset to 2.2 Å resolution was collected at RT from a 0.15 mm^3 PR_{TM}/KVS-1_{TI} crystal taken from the same crystallization drop that provided the crystal for room-temperature X-ray data on the LADI-III beamline at the Institut Laue-Langevin, Grenoble, France.[59] Images were collected from three different crystal orientations. At each orientation, the crystal was held stationary at different φ settings for each 24 h exposure. The neutron data were processed using the Daresbury Laboratory LAUE suite program LAUEGEN modified to account for the cylindrical geometry of the detector.[60,61] The program LSCALE[62] was used to determine the wavelength−normalization curve using the intensities of symmetry-equivalent reflections measured at different wavelengths. No explicit absorption corrections were applied. These data were then merged in SCALA.[63] The summary of experimental data statistics is given in Table S2.

Joint XN Refinement. The joint XN structure of the PR_{TM}/KVS-1_{TI} complex was determined using *nCNS*[42,64] and manipulated in *Coot*.[65] After initial rigid-body refinement, several cycles of positional, atomic displacement parameter and occupancy refinement were performed. The structure was checked for the correctness of side-chain conformations, hydrogen bonding, and orientation of D_2O water molecules, which were built based on the mFo-DFc difference neutron scattering length density maps. The 2mFo-DFc and mFo-DFc neutron scattering length density maps were then examined to determine the correct orientation of hydroxyl groups and

https://dx.doi.org/10.1021/acsomega.0c00835
ACS Omega 2020, 5, 11605−11617

protonation states of the enzyme residues. The protonation states of some disordered side chains could not be obtained directly and remained ambiguous. All water molecules were refined as D_2O. Initially, water oxygen atoms were positioned according to their electron density peaks and then were shifted slightly in accordance with the neutron scattering length density maps. All H atom positions in PR_{TM} and labile H positions in KVS-1_{TI} were modeled as D because of ∼85% deuteration level of the enzyme, and then the occupancies of the D atoms were refined individually within the range of −0.56 to 1.00. Before depositing the neutron structure to the PDB, a script was run that converts a record for the coordinates of a D atom into two records corresponding to an H and a D partially occupying the same site, both with positive partial occupancies that add up to unity.

Low and RT X-ray Refinement. The low-temperature X-ray structure of the PR_{TM}/KVS-1_{TI} complex was solved by molecular replacement using the structure in PDB (PDB ID: 3DCR)[43] as the search model in program *Phaser*, incorporated in *PHENIX*.[66] The Ramachandran statistics for the structures reported here have residues in most favored regions 98.5−99.0% and residues in additional allowed regions 1.5−1.0%. The RT X-ray structure of PR_{TM}/DRV_{TI} complex was solved by molecular replacement using the PR_{TM}/DRV structure (PDB ID: 5E5J)[46] and refined using SHELX-97.[67,68] Figures were generated using the PyMol molecular graphics software (Schrödinger LLC, v.2.2.0).

Cluster DFT and NBO Analysis. The cluster DFT model was constructed from the atomic positions extracted from our joint XN structure of the PR_{TM}/KVS-1_{TI} complex. The 194-atom model contained residues Asp25−Ala28, Asp25′−Ala28′, truncated Ile50 and Ile50′, the flap water, and truncated KVS-1_{TI} where all the side chains were reduced to methyl groups. All D atoms were renamed to H. All termini were capped with methyl acetamido groups and the methyl Hs were placed in idealized geometries with the program GaussView 6 from Gaussian (Wallingford, CT). The cluster model geometry was optimized at the M06-2X/6-311+G(d,p) level of theory along with the integral equation formalism variant of the polarizable continuum model (IEFPCM) for water solvation by using Gaussian 16, Revision B software from Gaussian.[69] During geometry optimizations of KVS-1_{TI} model in the oxyanion and *gem*-diol forms, positions of C, N, and O atoms were kept in their joint XN structure coordinates, while positions of H atoms were fully optimized. The optimized structures were subjected to natural bonding orbital analysis to identify the electron donor−acceptor interactions by a second-order perturbative analysis within the integrated Gaussian 16/NBO3.0 program.[70,71] Orbitals were depicted with GaussView 6.

QM/MM Calculations. The model was constructed using the atomic coordinates from the joint XN structure of the PR_{TM}/KVS-1_{TI} complex. 50 ps molecular dynamics simulations were first performed to equilibrate the model and the 11,141-atom model for QM/MM calculations was then constructed by retaining a 30 Å sphere of atoms centered around the hydroxyl oxygens of the KVS-1_{TI} inhibitor. Detailed description of these calculations is given in the Supporting Information and in Table S3.

ITC and Enzyme Activity Measurements. Stock solutions of the clinical inhibitor DRV (100 mM in DMSO) and keto-DRV (25 mM in DMSO) were diluted in a range of 90−150 μM in 5 mM sodium acetate, pH 6, and then adjusted to a final concentration with 50 mM sodium acetate, pH 5. ITC titrations were performed in 50 mM sodium acetate buffer at 28 °C and pH 5 on an ITC200 microcalorimeter (Malvern Instruments Inc., Westborough, MA) using 9−15 μM (as dimer) PR_{WT}, PR_{TM} or PR20, and 90−150 μM inhibitor. The PR samples were dialyzed against the ITC buffer in the presence of 0.36−0.6% DMSO prior to the measurements to compensate for the DMSO present in the titrant when diluting DRV or keto-DRV stock solutions. For competitive inhibitors that bind at only one site, dissociation constants ($K_d = 1/K_a$) are equivalent to the inhibition constants measured by enzyme kinetics (K_i). Data were processed using the Origin ITC software. Enzyme inhibition assays were carried out in 50 mM sodium acetate buffer (pH 5) at a final concentration of 0.5 μM mature PR either in the absence or presence of DRV or keto-DRV and 380 μM of the chromogenic substrate (Lys-Ala-Arg-Val-Nle-[4-nitrophenylalanine]-Glu-Ala-Nle-NH_2, California Peptide Research, Napa, CA) in a total volume of 120 μL at 28 °C.

PDB Depositions. Coordinates and structure factors have been deposited in the Protein Data Bank with the accession numbers: 6PTP for the RT joint XN structure of PR_{TM}/KVS-1_{TI}, 6KMP for the low-temperature X-ray structure of PR_{TM}/KVS-1_{TI}, and 6PU8 for RT X-ray structure of PR_{TM}/DRV_{TI}.

■ ASSOCIATED CONTENT

Supporting Information

The Supporting Information is available free of charge at https://pubs.acs.org/doi/10.1021/acsomega.0c00835.

Details of the QM/MM calculations, sequence alignment of PR_{WT}, PR_{TM}, and PR_{20}, crystallographic data collection and refinement statistics, distances (Å) from C(KVS-1) to O(W_{cat}) in QM/MM calculations, electron density of KVS-1_{TI}, comparison of the joint XN structure with unliganded HIV-1 PR and PR_{I54V}/TI, Figures 4A,B and 5B in crossed-eye stereo mode, comparison of the room- and low-temperature structures of the PR_{TM}/KVS-1_{TI} complex, catalytic site geometries from QM/MM calculations, comparison of PR_{TM}/DRV_{TI} and PR_{TM}/DRV complexes, raw ITC plots, and the effect of DRV and keto-DRV on PR variant substrate hydrolysis (PDF)

■ AUTHOR INFORMATION

Corresponding Authors

Amit Das − *Protein Crystallography Section, Radiation Biology and Health Sciences Division, Bhabha Atomic Research Centre, Mumbai 400085, India; Homi Bhabha National Institute, Mumbai 400094, India*; Email: amitdas@barc.gov.in

Andrey Kovalevsky − *Neutron Scattering Division, Oak Ridge National Laboratory, Oak Ridge, Tennessee 37830, United States*; orcid.org/0000-0003-4459-9142; Email: kovalevskyay@ornl.gov

Authors

Mukesh Kumar − *Protein Crystallography Section, Radiation Biology and Health Sciences Division, Bhabha Atomic Research Centre, Mumbai 400085, India; Homi Bhabha National Institute, Mumbai 400094, India*

Kalyaneswar Mandal − *Departments of Chemistry, and Biochemistry and Molecular Biology, Institute for Biophysical*

https://dx.doi.org/10.1021/acsomega.0c00835
ACS Omega 2020, 5, 11605−11617

Dynamics, University of Chicago, Chicago, Illinois 60637, United States; orcid.org/0000-0002-3194-1378

Matthew P. Blakeley − *Large Scale Structures Group, Institut Laue−Langevin, 38000 Grenoble, France;* orcid.org/0000-0002-6412-4358

Troy Wymore − *Department of Chemistry, University of Michigan, Ann Arbor, Michigan 48109, United States;* orcid.org/0000-0003-1969-2652

Stephen B. H. Kent − *Departments of Chemistry, and Biochemistry and Molecular Biology, Institute for Biophysical Dynamics, University of Chicago, Chicago, Illinois 60637, United States*

John M. Louis − *Laboratory of Chemical Physics, National Institute of Diabetes and Digestive and Kidney Diseases, National Institutes of Health, DHHS, Bethesda, Maryland 20892-0520, United States*

Complete contact information is available at: https://pubs.acs.org/10.1021/acsomega.0c00835

Author Contributions

A.D. designed research and planned experiments; A.D. and A.K. performed research; A.D. and M.P.B. collected neutron diffraction data; A.D., K.M., and A.K. collected X-ray diffraction data; A.D., A.K., K.M., M.K., M.P.B., and S.B.H.K. analyzed the data and results; A.K. and T.W. performed molecular modeling; J.M.L. collected and analyzed ITC and the enzyme kinetics data; and A.D., J.M.L., and A.Y.K. wrote the manuscript with input from all authors.

Notes

The authors declare no competing financial interest.

■ ACKNOWLEDGMENTS

This research using IMAGINE beamline at the Oak Ridge National Laboratory's (ORNL) High Flux Isotope Reactor (HFIR) was sponsored by the Scientific User Facilities Division, Office of Basic Energy Sciences, U.S. Department of Energy. This research was supported by the Protein Crystallography Section, RB & HSD at Bhabha Atomic Research Centre (BARC), Mumbai, and by the Office of Biological and Environmental Research at Oak Ridge National Laboratory's Center for Structural Molecular Biology (CSMB). We used facilities supported by the Scientific User Facilities Division, Office of Basic Energy Sciences, U.S. Department of Energy and National Facility for Structural Biology, Department of Atomic Energy (DAE, India). We thank Institut Laue-Langevin (ILL, Grenoble, France) for awarding neutron beamtime on neutron diffraction beamline LADI-III. The D_2O used in this research was supplied by the United States Department of Energy Office of Science by the Isotope Program in the Office of Nuclear Physics. We thank beamline staff of LADI-III, and 5.0.3 beamline at BCSB, Advanced Light Source, Lawrence Berkeley National Laboratory, California, USA for their support. We also thank the Department of Science and Technology, France Embassy, New Delhi for travel support to ILL and Dr. R. Chidambaram (DAE), former Principal Scientific Advisor to the Government of India for discussions. A.D. was supported by BARC, DAE. A.K. was supported by DOE BES. We also acknowledge support from the National Institute of Diabetes and Digestive and Kidney Diseases, National Institutes of Health. This manuscript has been authored jointly by DAE, BARC, India and UT-Battelle LLC under DOE contract no. DE-AC05-00OR22725.

■ REFERENCES

(1) Engelman, A.; Cherepanov, P. The Structural Biology of HIV-1: Mechanistic and Therapeutic Insights. *Nat. Rev. Microbiol.* **2012**, *10*, 279−290.

(2) Hartman, T. L.; Buckheit, R. W., Jr. The Continuing Evolution of HIV-1 Therapy: Identification and Development of Novel Antiretroviral Agents Targeting Viral and Cellular Targets. *Mol. Biol. Int.* **2012**, *2012*, 401965.

(3) Wensing, A. M. J.; van Maarseveen, N. M.; Nijhuis, M. Fifteen Years of HIV Protease Inhibitors: Raising the Barrier to Resistance. *Antiviral Res.* **2010**, *85*, 59−74.

(4) Mitsuya, H.; Maeda, K.; Das, D.; Ghosh, A. K. Development of Protease Inhibitors and the Fight with Drug-Resistant HIV-1 Variants. *Adv. Pharmacol.* **2008**, *56*, 169−197.

(5) Ghosh, A. K.; Osswald, H. L.; Prato, G. Recent Progress in the Development of HIV-1 Protease Inhibitors for the Treatment of HIV/AIDS. *J. Med. Chem.* **2016**, *59*, 5172−5208.

(6) Subbaiah, M. A. M.; Meanwell, N. A.; Kadow, J. F. Design Strategies in the Prodrugs of HIV-1 Protease Inhibitors to Improve the Pharmaceutical Properties. *Eur. J. Med. Chem.* **2017**, *139*, 865−883.

(7) Weber, I.; Harrison, RW Tackling the Problem of HIV Drug Resistance. *Postepy Biochem.* **2016**, *62*, 273−279.

(8) Beck, Z.; Morris, G.; Elder, J. Defining HIV-1 Protease Substrate Selectivity. *Curr. Drug Targets* **2002**, *2*, 37−50.

(9) Navia, M. A.; Fitzgerald, P. M. D.; McKeever, B. M.; Leu, C.-T.; Heimbach, J. C.; Herber, W. K.; Sigal, I. S.; Darke, P. L.; Springer, J. P. Three-Dimensional Structure of Aspartyl Protease from Human Immunodeficiency Virus HIV-1. *Nature* **1989**, *337*, 615−620.

(10) Wlodawer, A.; Miller, M.; Jaskolski, M.; Sathyanarayana, B.; Baldwin, E.; Weber, I.; Selk, L.; Clawson, L.; Schneider, J.; Kent, S. Conserved Folding in Retroviral Proteases: Crystal Structure of a Synthetic HIV-1 Protease. *Science* **1989**, *245*, 616−621.

(11) Lapatto, R.; Blundell, T.; Hemmings, A.; Overington, J.; Wilderspin, A.; Wood, S.; Merson, J. R.; Whittle, P. J.; Danley, D. E.; Geoghegan, K. F.; Hawrylik, S. J.; Lee, S. E.; Scheld, K. G.; Hobart, P. M. X-ray Analysis of HIV-1 Proteinase at 2.7 Å Resolution Confirms Structural Homology Among Retroviral Enzymes. *Nature* **1989**, *342*, 299−302.

(12) *Aspartic Acid Proteases as Therapeutic Targets*; Ghosh, A. K., Ed.; Wiley-CVH Verlag GmbH & Co. KGaA, 2010; Vol. *45*, p 615.

(13) Brik, A.; Wong, C.-H. HIV-1 Protease: Mechanism and Drug Discovery. *Org. Biomol. Chem.* **2003**, *1*, 5−14.

(14) Hyland, L. J.; Tomaszek, T. A., Jr.; Roberts, G. D.; Carr, S. A.; Magaard, V. W.; Bryan, H. L.; Fakhoury, S. A.; Moore, M. L.; Minnich, M. D.; Culp, J. S.; DesJarlais, R. L.; Meek, T. D. Human Immunodeficiency Virus-1 Protease: 1. Initial Velocity Studies and Kinetic Characterization of Reaction Intermediates by ^{18}O Isotope Exchange. *Biochemistry* **1991**, *30*, 8441−8453.

(15) Hyland, L. J.; Tomaszek, T. A., Jr.; Meek, T. D. Human Immunodeficiency Virus-1 Protease: 2. Use of pH Rate Studies and Solvent Kinetic Isotope Effects to Elucidate Details of Chemical Mechanism. *Biochemistry* **1991**, *30*, 8454−8463.

(16) Northrop, D. B. Follow the Protons: A Low-Barrier Hydrogen Bond Unifies the Mechanisms of the Aspartic Proteases. *Acc. Chem. Res.* **2001**, *34*, 790−797.

(17) Kipp, D. R.; Hirschi, J. S.; Wakata, A.; Goldstein, H.; Schramm, V. L. Transition States of Native and Drug-Resistant HIV-1 Protease are the Same. *Proc. Natl. Acad. Sci. U.S.A.* **2012**, *109*, 6543−6548.

(18) Torbeev, V. Y.; Kent, S. B. H. Ionization State of the Catalytic Dyad Asp25/25' in the HIV-1 Protease: NMR Studies of Site-Specifically ^{13}C Labelled HIV-1 Protease Prepared by Total Chemical Synthesis. *Org. Biomol. Chem.* **2012**, *10*, 5887−5891.

(19) Rodriguez, E. J.; Angeles, T. S.; Meek, T. D. Use of Nitrogen-15 Kinetic Isotope Effects to Elucidate Details of the Chemical Mechanism of Human Immunodeficiency Virus 1 Protease. *Biochemistry* **1993**, *32*, 12380−12385.

(20) Torshin, I. Y.; Harrison, R. W.; Weber, I. T. Close Pairs of Carboxylates: a Possibility of Multicenter Hydrogen Bonds in Proteins. *Protein Eng.* **2003**, *16*, 201−207.
(21) Piana, S.; Carloni, P. Conformational Flexibility of the Catalytic Asp Dyad in HIV-1 Protease: an Ab Initio Study on the Free Enzyme. *Proteins: Struct., Funct., Genet.* **2000**, *39*, 26−36.
(22) Porter, M. A.; Molina, P. A. The Low-Barrier Double-Well Potential of the Oδ1-H-Oδ1 Hydrogen Bond in Unbound HIV Protease: a QM/MM Characterization. *J. Chem. Theory Comput.* **2006**, *2*, 1675−1684.
(23) Chatfield, D. C.; P. Eurenius, K.; Brooks, B. R. HIV-1 Protease Cleavage Mechanism: a Theoretical Investigation Based on Classical MD Simulation and Reaction Path Calculations Using a Hybrid QM/MM Potential. *J. Mol. Struct.* **1998**, *423*, 79−92.
(24) Okimoto, N.; Tsukui, T.; Hata, M.; Hoshino, T.; Tsuda, M. Hydrolysis Mechanism of the Phenylalanine-Proline Peptide Bond Specific to HIV-1 Protease: Investigation by the Ab Initio Molecular Orbital Method. *J. Am. Chem. Soc.* **1999**, *121*, 7349−7354.
(25) Piana, S.; Carloni, P.; Parrinello, M. Role of Conformational Fluctuations in the Enzymatic Reaction of HIV-1 Protease. *J. Mol. Biol.* **2002**, *319*, 567−583.
(26) Piana, S.; Bucher, D.; Carloni, P.; Rothlisberger, U. Reaction Mechanism of HIV-1 Protease by Hybrid Car-Parrinello/Classical MD Simulations. *J. Phys. Chem. B* **2004**, *108*, 11139−11149.
(27) Trylska, J.; Grochowski, P.; McCammon, J. A. The Role of Hydrogen Bonding in the Enzymatic Reaction Catalyzed by HIV-1 Protease. *Protein Sci.* **2004**, *13*, 513−528.
(28) Bjelic, S.; Åqvist, J. Catalysis and Linear Free Energy Relationships in Aspartic Proteases. *Biochemistry* **2006**, *45*, 7709−7723.
(29) Garrec, J.; Sautet, P.; Fleurat-Lessard, P. Understanding the HIV-1 Protease Reactivity with DFT: What Do We Gain from Recent Functionals? *J. Phys. Chem. B* **2011**, *115*, 8545−8558.
(30) Ribeiro, A. J. M.; Santos-Martins, D.; Russo, N.; Ramos, M. J.; Fernandes, P. A. Enzymatic Flexibility and Reaction Rate: a QM/MM Study of HIV-1 Protease. *ACS Catal.* **2015**, *5*, 5617−5626.
(31) Krzeminska, A.; Moliner, V.; Swiderek, K. Dynamic and Electrostatic Effects on the Reaction Catalyzed by HIV-1 Protease. *J. Am. Chem. Soc.* **2016**, *138*, 16283−16298.
(32) Thacker, J. C. R.; Vincent, M. A.; Popelier, P. L. A. Using the Relative Energy Gradient Method with Interacting Quantum Atoms to Determine the Reaction Mechanism and Catalytic Effects in the Peptide Hydrolysis in HIV-1 Protease. *Chem.—Eur. J.* **2018**, *24*, 11200−11210.
(33) Sadiq, S. K.; Coveney, P. V. Computing the Role of Near Attack Conformations in an Enzyme-Catalyzed Nucleophilic Bimolecular Reaction. *J. Chem. Theory Comput.* **2015**, *11*, 316−324.
(34) Lawal, M. M.; Sanusi, Z. K.; Govender, T.; Tolufashe, G. F.; Maguire, G. E. M.; Honarparvar, B.; Kruger, H. G. Unraveling the Concerted Catalytic Mechanism of the Human Immunodeficiency Virus Type 1 (HIV-1) Protease: a Hybrid QM/MM Study. *Struct. Chem.* **2019**, *30*, 409−417.
(35) Slee, D. H.; Laslo, K. L.; Elder, J. H.; Ollmann, I. R.; Gustchina, A.; Kervinen, J.; Zdanov, A.; Wlodawer, A.; Wong, C.-H. Selectivity in the Inhibition of HIV and FIV Protease: Inhibitory and Mechanistic Studies of Pyrrolidine-Containing α-Keto Amide and Hydroxyethyleneamine Core Structures. *J. Am. Chem. Soc.* **1995**, *117*, 11867−11878.
(36) Silva, A. M.; Cachau, R. E.; Sham, H. L.; Erickson, J. W. Inhibition and Catalytic Mechanism of HIV-1 Aspartic Protease. *J. Mol. Biol.* **1996**, *255*, 321−340.
(37) Kovalevsky, A. Y.; Chumanevich, A. A.; Liu, F.; Louis, J. M.; Weber, I. T. Caught in the Act: the 1.5 Å Resolution Crystal Structures of the HIV-1 Protease and the I54V Mutant Reveal a Tetrahedral Reaction Intermediate. *Biochemistry* **2007**, *46*, 14854−14864.
(38) Das, A.; Mahale, S.; Prashar, V.; Bihani, S.; Ferrer, J.-L.; Hosur, M. V. X-ray Snapshot of HIV-1 Protease in Action: Observation of Tetrahedral Intermediate and Short Ionic Hydrogen Bond SIHB with Catalytic Aspartate. *J. Am. Chem. Soc.* **2010**, *132*, 6366−6373.
(39) Shen, C.-H.; Tie, Y.; Yu, X.; Wang, Y.-F.; Kovalevsky, A. Y.; Harrison, R. W.; Weber, I. T. Capturing the Reaction Pathway in Near-Atomic-Resolution Crystal Structures of HIV-1 Protease. *Biochemistry* **2012**, *51*, 7726−7732.
(40) Oksanen, E.; Chen, J. C.-H.; Fisher, S. Z. Neutron Crystallography for the Study of Hydrogen Bonds in Macromolecules. *Molecules* **2017**, *22*, 596.
(41) Ashkar, R.; Bilheux, H. Z.; Bordallo, H.; Briber, R.; Callaway, D. J. E.; Cheng, X.; Chu, X.-Q.; Curtis, J. E.; Dadmun, M.; Fenimore, P.; Fushman, D.; Gabel, F.; Gupta, K.; Herberle, F.; Heinrich, F.; Hong, L.; Katsaras, J.; Kelman, Z.; Kharlampieva, E.; Kneller, G. R.; Kovalevsky, A.; Krueger, S.; Langan, P.; Lieberman, R.; Liu, Y.; Losche, M.; Lyman, E.; Mao, Y.; Marino, J.; Mattos, C.; Meilleur, F.; Moody, P.; Nickels, J. D.; O'Dell, W. B.; O'Neill, H.; Perez-Salas, U.; Peters, J.; Petridis, L.; Sokolov, A. P.; Stanley, C.; Wagner, N.; Weinrich, M.; Weiss, K.; Wymore, T.; Zhang, Y.; Smith, J. C. Neutron Scattering in the Biological Sciences: Progress and Prospects. *Acta Crystallogr., Sect. D: Struct. Biol.* **2018**, *74*, 1129−1168.
(42) Adams, P. D.; Mustyakimov, M.; Afonine, P. V.; Langan, P. Generalized X-ray and Neutron Crystallographic Analysis: More Accurate and Complete Structures for Biological Macromolecules. *Acta Crystallogr., Sect. D: Biol. Crystallogr.* **2009**, *65*, 567−573.
(43) Torbeev, V. Y.; Mandal, K.; Terechko, V. A.; Kent, S. B. H. Crystal Structure of Chemically Synthesized HIV-1 Protease and a Ketomethylene Isostere Inhibitor Based on the p2/NC Cleavage Site. *Bioorg. Med. Chem. Lett.* **2008**, *18*, 4554−4557.
(44) Torbeev, V. Y.; Raghuraman, H.; Hamelberg, D.; Tonelli, M.; Westler, W. M.; Perozo, E.; Kent, S. B. H. Protein Conformational Dynamics in the Mechanism of HIV-1 Protease Catalysis. *Proc. Natl. Acad. Sci. U.S.A.* **2011**, *108*, 20982−20987.
(45) Gerlits, O.; Keen, D. A.; Blakeley, M. P.; Louis, J. M.; Weber, I. T.; Kovalevsky, A. Room Temperature Neutron Crystallography of Drug Resistant HIV-1 Protease Uncovers Limitations of X-ray Structure Analysis at 100K. *J. Med. Chem.* **2017**, *60*, 2018−2025.
(46) Gerlits, O.; Wymore, T.; Das, A.; Shen, C.-H.; Parks, J. M.; Smith, J. C.; Weiss, K. L.; Keen, D. A.; Blakeley, M. P.; Louis, J. M.; Langan, P.; Weber, I. T.; Kovalevsky, A. Long-Range Electrostatics-Induced Two-Proton Transfer Captured by Neutron Crystallography in an Enzyme Catalytic Site. *Angew. Chem., Int. Ed.* **2016**, *55*, 4924−4927.
(47) Steiner, T. The hydrogen bond in the solid state. *Angew. Chem., Int. Ed.* **2002**, *41*, 49−76.
(48) Windsor, I. W.; Gold, B.; Raines, R. T. An n→π* Interaction in the Bound Substrate of Aspartic Proteases Replicates the Oxyanion Hole. *ACS Catal.* **2019**, *9*, 1464−1471.
(49) Marinier, A.; Toth, M. V.; Houseman, K.; Mueller, R.; Marshall, G. R. HIV-1 Protease Inhibitors: Ketomethylene Isosteres with Unusually High Affinity Compared with Hydroxyethylene Isostere Analogs. *Bioorg. Med. Chem.* **1994**, *2*, 919−925.
(50) Sayer, J. M.; Liu, F.; Ishima, R.; Weber, I. T.; Louis, J. M. Effect of the Active Site D25N Mutation on the Structure, Stability, and Ligand Binding of the Mature HIV-1 Protease. *J. Biol. Chem.* **2008**, *283*, 13459−13470.
(51) Louis, JM; Clore, GM; Gronenborn, AM Autoprocessing of HIV-1 Protease is Tightly Coupled to Protein Folding. *Nat. Struct. Biol.* **1999**, *6*, 868−75.
(52) Wondrak, E. M.; Louis, J. M. Influence of Flanking Sequences on the Dimer Stability of Human Immunodeficiency Virus Type 1 Protease. *Biochemistry* **1996**, *35*, 12957−12962.
(53) Mahalingam, B.; Louis, J. M.; Hung, J.; Harrison, R. W.; Weber, I. T. Structural Implications of Drug-Resistant Mutants of HIV-1 Protease: High-Resolution Crystal Structures of the Mutant Protease/Substrate Analogue Complexes. *Proteins: Struct., Funct., Genet.* **2001**, *43*, 455−464.
(54) Louis, J. M.; Aniana, A.; Weber, I. T.; Sayer, J. M. Inhibition of Autoprocessing of Natural Variants and Multidrug Resistant Mutant

https://dx.doi.org/10.1021/acsomega.0c00835
ACS Omega 2020, 5, 11605−11617

Precursors of HIV-1 Protease by Clinical Inhibitors. *Proc. Natl. Acad. Sci. U.S.A.* **2011**, *108*, 9072−9077.
(55) Weber, I. T.; Waltman, M. J.; Mustyakimov, M.; Blakeley, M. P.; Keen, D. A.; Ghosh, A. K.; Langan, P.; Kovalevsky, A. Y. Joint X-ray/Neutron Crystallographic Study of HIV-1 Protease with Clinical Inhibitor Amprenavir: Insights for Drug Design. *J. Med. Chem.* **2013**, *56*, 5631−5635.
(56) Minor, W.; Cymborowski, M.; Otwinowski, Z.; Chruszcz, M. HKL3000: The Integration of Data, Reduction and Structure Solution − From Diffraction Images to an Initial Model in Minutes. *Acta Crystallogr., Sect. D: Biol. Crystallogr.* **2006**, *62*, 859−866.
(57) Battye, T. G. G.; Kontogiannis, L.; Johnson, O.; Powell, H. R.; Leslie, A. G. W. IMosflm: a New Graphical Interface for Diffraction-Image Processing with MOSFLM. *Acta Crystallogr., Sect. D: Biol. Crystallogr.* **2011**, *67*, 271−281.
(58) Meilleur, F.; Munshi, P.; Robertson, L.; Stoica, A. D.; Crow, L.; Kovalevsky, A.; Koritsanszky, T.; Chakoumakos, B. C.; Blessing, R.; Myles, D. A. A. The IMAGINE instrument: first neutron protein structure and new capabilities for neutron macromolecular crystallography. *Acta Crystallogr., Sect. D: Biol. Crystallogr.* **2013**, *69*, 2157−2160.
(59) Blakeley, M. P.; Teixeira, S. C. M.; Petit-Haertlein, I.; Hazemann, I.; Mitschler, A.; Haertlein, M.; Howard, E.; Podjarny, A. D. Neutron Macromolecular Crystallography with LADI-III. *Acta Crystallogr., Sect. D: Biol. Crystallogr.* **2010**, *66*, 1198−1205.
(60) Campbell, J. W. LAUEGEN, an X-Windows-Based Program for the Processing of Laue Diffraction Data. *J. Appl. Crystallogr.* **1995**, *28*, 228−236.
(61) Campbell, J. W.; Hao, Q.; Harding, M. M.; Nguti, N. D.; Wilkinson, C. LAUEGEN Version 6.0 and INTLDM. *J. Appl. Crystallogr.* **1998**, *31*, 496−502.
(62) Arzt, S.; Campbell, J. W.; Harding, M. M.; Hao, Q.; Helliwell, J. R. LSCALE - the New Normalization, Scaling and Absorption Correction Program in the Daresbury Laue Software Suite. *J. Appl. Crystallogr.* **1999**, *32*, 554−562.
(63) Weiss, M. S. Global Indicators of X-ray Data Quality. *J. Appl. Crystallogr.* **2001**, *34*, 130−135.
(64) Mustyakimov, M.; Langan, P. *Copyright C-06, 104 Patch for CNS; nCNS an Open Source Distribution Patch for CNS for Macromolecular Structure Refinement*; Los Alamos National Security: Los Alamos, NM, USA, 2007.
(65) Emsley, P.; Lohkamp, B.; Scott, W. G.; Cowtan, K. Features and Development of Coot. *Acta Crystallogr., Sect. D: Biol. Crystallogr.* **2010**, *66*, 486−501.
(66) Adams, P. D.; Afonine, P. V.; Bunkóczi, G.; Chen, V. B.; Davis, I. W.; Echols, N.; Headd, J. J.; Hung, L.-W.; Kapral, G. J.; Grosse-Kunstleve, R. W.; McCoy, A. J.; Moriarty, N. W.; Oeffner, R.; Read, R. J.; Richardson, D. C.; Richardson, J. S.; Terwilliger, T. C.; Zwart, P. H. PHENIX: a Comprehensive Python-Based System for Macromolecular Structure Solution. *Acta Crystallogr., Sect. D: Biol. Crystallogr.* **2010**, *66*, 213−221.
(67) Sheldrick, G. M. Short History of SHELX. *Acta Crystallogr., Sect. A: Found. Crystallogr.* **2008**, *64*, 112−122.
(68) Sheldrick, G. M. Crystal Structure Refinement with SHELXL. *Acta Crystallogr., Sect. C: Struct. Chem.* **2015**, *71*, 3−8.
(69) Frisch, M. J.; Trucks, G. W.; Schlegel, H. B.; Scuseria, G. E.; Robb, M. A.; Cheeseman, J. R.; Scalmani, G.; Barone, V.; Petersson, G. A.; Nakatsuji, H.; Li, X.; Caricato, M.; Marenich, A. V.; Bloino, J.; Janesko, B. G.; Gomperts, R.; Mennucci, B.; Hratchian, H. P.; Ortiz, J. V.; Izmaylov, A. F.; Sonnenberg, J. L.; Williams-Young, D.; Ding, F.; Lipparini, F.; Egidi, F.; Goings, J.; Peng, B.; Petrone, A.; Henderson, T.; Ranasinghe, D.; Zakrzewski, V. G.; Gao, J.; Rega, N.; Zheng, G.; Liang, W.; Hada, M.; Ehara, M.; Toyota, K.; Fukuda, R.; Hasegawa, J.; Ishida, M.; Nakajima, T.; Honda, Y.; Kitao, O.; Nakai, H.; Vreven, T.; Throssell, K.; Montgomery, J. A., Jr.; Peralta, J. E.; Ogliaro, F.; Bearpark, M. J.; Heyd, J. J.; Brothers, E. N.; Kudin, K. N.; Staroverov, V. N.; Keith, T. A.; Kobayashi, R.; Normand, J.; Raghavachari, K.; Rendell, A. P.; Burant, J. C.; Iyengar, S. S.; Tomasi, J.; Cossi, M.; Millam, J. M.; Klene, M.; Adamo, C.; Cammi, R.; Ochterski, J. W.; Martin, R. L.; Morokuma, K.; Farkas, O.; Foresman, J. B.; Fox, D. J. *Gaussian 16*, Revision A.03; Gaussian, Inc.: Wallingford, CT, 2016.
(70) Reed, A. E.; Weinstock, R. B.; Weinhold, F. Natural population analysis. *J. Chem. Phys.* **1985**, *83*, 735−746.
(71) Glendening, E.; Reed, A.; Carpenter, J.; Weinhold, F. *NBO Program*, version 3.1; University of Wisconsin: Madison 2001.
(72) King, N. M.; Prabu-Jeyabalan, M.; Nalivaika, E. A.; Wigerinck, P.; de Béthune, M.-P.; Schiffer, C. A. Structural and Thermodynamic Basis for the Binding of TMC114, a Next-Generation Human Immunodeficiency Virus Type 1 Protease Inhibitor. *J. Virol.* **2004**, *78*, 12012−12021.

https://dx.doi.org/10.1021/acsomega.0c00835
ACS Omega 2020, 5, 11605−11617